Effects of sheet resistance and contact shading on the characterization of solar cells by open-circuit voltage measurements

N.-P. Harder[a] and A. B. Sproul
Centre for Photovoltaic Engineering, University of New South Wales, Sydney 2052, New South Wales, Australia

T. Brammer
Institute of Photovoltaics, Forschungszentrum Jülich, Germany

A. G. Aberle
Centre for Photovoltaic Engineering, University of New South Wales, Sydney 2052, New South Wales, Australia

(Received 14 March 2003; accepted 6 June 2003)

The measurement of the open-circuit voltage (V_{oc}) as a function of the illumination intensity (Suns–V_{oc}) is a useful tool for characterizing solar cells, giving a characteristic curve with virtually no influence from series resistance. In particular, Suns–V_{oc} measurements allow the extraction of the diode properties without a complete contacting scheme, such as for test structures in research or for quality control between processing steps during production. In this article, we show by means of resistive network calculations, that the combination of contact shading and high sheet resistance can cause severe deviations of the measured Suns–V_{oc} curve from that measured without contact shading or with only negligible sheet resistance. These deviations bear the danger of an erroneous assessment of the fundamental diode properties. For sheet resistances typical for thin layers of doped hydrogenated amorphous Si even the shadow of the tip of a needle-shaped contacting probe can be sufficient to cause a distorted Suns–V_{oc} curve. Results of experiments performed on a microcrystalline $p-i-n$ Si thin-film solar cell with an amorphous n layer are presented and qualitatively explained within the framework of a resistive network model. A ''rule of thumb'' is presented, which allows an estimate to be made of the impact of contact shading and sheet resistance on V_{oc} measurements for arbitrary solar cells and contact area sizes. © *2003 American Institute of Physics.* [DOI: 10.1063/1.1595141]

I. INTRODUCTION

Measuring the short-circuit current density (J_{sc}) and the open-circuit voltage (V_{oc}) for a range of illumination levels is a well-known procedure for characterizing the fundamental diode properties of solar cells [$J_{sc}-V_{oc}$ method (Ref. 1)] with virtually no influence of (moderate) series resistance values. For very high series resistance, however, the $J_{sc}-V_{oc}$ pairs can vary significantly from the current–voltage ($I-V$) curve in the absence of series resistance. In such cases, monitoring the light intensity with a separate device (e.g., a calibrated reference solar cell), instead of measuring the J_{sc}, yields the characteristic curve, a ''Suns–V_{oc}'' curve, without influence from series resistance.[1–3]

In most cases the $I-V$ curve under illumination (light $I-V$ curve) can be expressed as a superposition of the (dark) $I-V$ curve with the light-generated current I_L,

$$I(V)=I_0\left(\exp\left(\frac{V-I(V)\times R_s}{mV_T}\right)-1\right)+\frac{V-I(V)\times R_s}{R_{sh}}-I_L, \tag{1}$$

where I_0 is the saturation current, R_s the series resistance, R_{sh} the shunt resistance, m the ideality factor, and V_T the thermal voltage. In the Suns–V_{oc} method only the open-circuit voltage (V_{oc}) is measured, that is $I(V_{oc})=0$. The illumination density Φ is proportional to the light-generated current density, and thus the Suns–V_{oc} curve is given as

$$\Phi\propto I_L=I_0\left(\exp\left(\frac{V_{oc}}{mV_T}\right)-1\right)+\frac{V_{oc}}{R_{sh}}. \tag{2}$$

The Suns–V_{oc} curve [Eq. (2)] is, therefore, equivalent to the dark $I-V$ curve, for the case where the series resistance R_s is zero. This curve only depends on the properties of the diode via I_0 and m, as well as the parasitic shunt resistance R_{sh}.

A convenient way of obtaining Suns–V_{oc} curves in quasi-steady-state measurements is illustrated in Fig. 1,[2] with a detailed analysis of the method given in Ref. 3. A flash lamp with a slowly decaying light intensity ($\tau_{pulse}=1$ ms) is used for illuminating the sample. A digital oscilloscope records the open-circuit voltage of the solar cell simultaneously with the I_{sc} of a calibrated reference cell, with the latter signal being a measure of the light intensity.

A consequence (and benefit) of the insensitivity towards series resistance is that the Suns–V_{oc} method does not require an optimized contacting scheme. In many cases simply pressing a metal probe onto the doped region is a sufficient

[a]Author to whom correspondence should be addressed; electronic mail:n.harder@unsw.edu.au

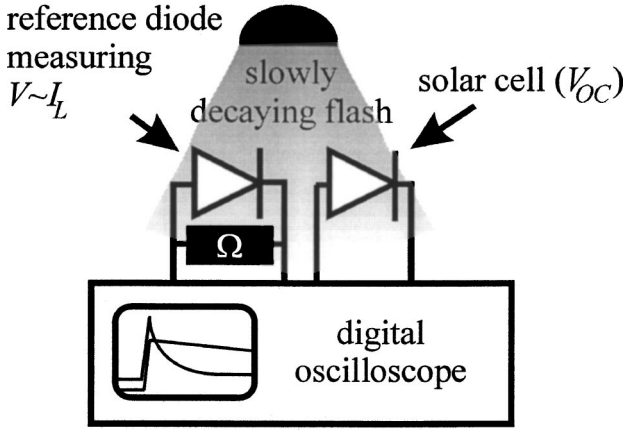

FIG. 1. Suns–V_{oc} measurement setup used for the experiments of this work. The setup is discussed in detail in Refs. 2 and 3.

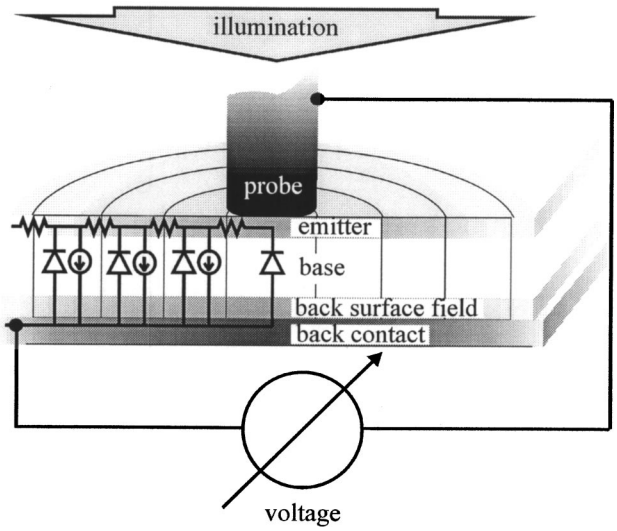

FIG. 2. Cross-sectional schematic representation of the resistive network model used for simulating the distortion of Suns–V_{oc} curves in the presence of contact shading and high sheet resistance. The metal probe for measuring the voltage shades the underlying region if illuminated from the side of the contact. The back surface of the solar cell is covered with a highly conductive contact layer (e.g., a metal back contact).

contact. By utilizing a preamplifier with very high input impedance the fundamental diode properties can even be determined in the presence of high contact resistance.[4] This makes the Suns–V_{oc} method very attractive for characterizing test structures in research or for quality control in production before the application of metallisation.

In this article, we use a simple resistive network model to show that despite the ruggedness of the Suns–V_{oc} method towards series resistance and crude contacting, the combination of high sheet resistance with contact shading can significantly distort the diode characteristics obtained from Suns–V_{oc} measurements. For sheet resistances typical for thin layers of doped hydrogenated amorphous Si (a-Si:H), even the shadow of the tip of a needle shaped probe for contacting can be sufficient to cause a distorted Suns–V_{oc} curve. Results of experiments on a $p-i-n$ thin-film solar cell consisting of p-type and intrinsic (''i''-type) layers of hydrogenated microcrystalline silicon (μc-Si:H) and an n layer of highly doped a-Si:H are presented and qualitatively explained within the framework of the resistive network model. Further details of μc-Si:H $p-i-n$ thin-film solar cells similar to those examined in this paper have been published elsewhere.[5,6]

II. RESISTIVE NETWORK

A. Model

Figure 2 shows a schematic representation of the resistive network model (similar to that of Ref. 7, for example) used to describe the combined effect of high sheet resistance and contact shading. The terminology indicated in Fig. 2 is that, typically, used for conventional $p-n$ junction solar cells, in which the ''emitter'' and the ''back surface field'' are highly doped layers of opposite types and the ''base'' is the (lightly doped) main absorber. In $p-i-n$ solar cells the main absorber is ''intrinsic,'' i.e., not intentionally doped. Despite of the fact that the electrical characteristics of $p-i-n$ junction diodes are drift-current dominated and that of $p-n$ junction diodes diffusion-current dominated, the model is described and discussed for both types of diodes simultaneously. This can be done as the model does not depend on the microscopic current mechanisms and makes only use of the exponential dependence of the current on the external voltage, which is the case for both types of diodes.

In Fig. 2, the contact to the emitter is sketched as a probe (this could also be an evaporated contact pad). In the model, the probe contacts the entire surface area that it is shading. Lateral flows of current in the emitter are impeded by the sheet resistance of the emitter, sketched as resistors in Fig. 2. The same applies to the backside of the solar cell. However, it is assumed that the back contact of the solar cell is highly conductive, i.e., has only negligible sheet resistance. Correspondingly, in the equivalent circuit shown in Fig. 2 the backcontact is represented as a connection without resistors between the individual diodes and current sources.

In the case where there is no shading, there is no lateral variation in the voltage across the diode. In this case, the voltage measured across the $p-n$ (or $p-i-n$) junction is simply the photogenerated voltage, which results form balancing the light-generated current and the recombination current (including shunt current, if applicable). That is, in the absence of localized contact shading (or other lateral inhomogeneities), the only current flows occur perpendicularly to the junction.

However, in the presence of (localized) contact shading lateral flow of current has to occur. In the model, it is assumed that the current flow in the lowly doped (or even ''intrinsic'') absorber still occurs perpendicularly to the junction while the only lateral flow of current occurs in the highly conductive backcontact and the highly doped emitter. For the open-circuit conditions considered in this article, this assumption is in agreement with the results of two-dimensional simulations of microcrystalline $p-i-n$ junctions of Fantoni *et al.*[8] Conditions under which this assumption may break down are discussed later in this section.

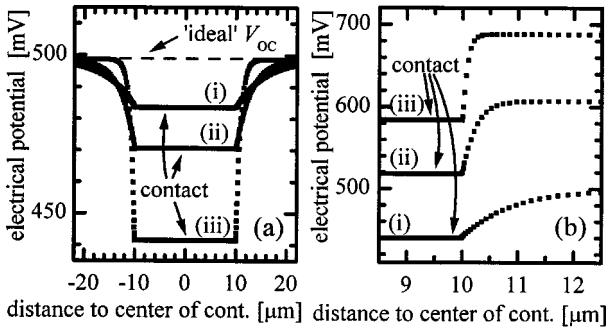

FIG. 3. Calculated example of the spatial voltage distribution under "open-circuit conditions" in the presence of contact shading and high sheet resistivity. (a) Light-generated current density at 1 Sun $j_L = 15$ mA cm^{-2}. Sheet resistance values (Ω/sq): (i) 6×10^6, (ii) 3×10^7, and (iii) 4.5×10^8. (b): Sheet resistance: 4.5×10^8 Ω/sq 1-Sun j_L values (mA cm^{-2}): (i) 15, (ii) 240, and (iii) 1875. It is assumed that the contact shading is not complete, i.e., the average light-generated current density in the volume under the contact is assumed to be 5% of that in the surrounding area.

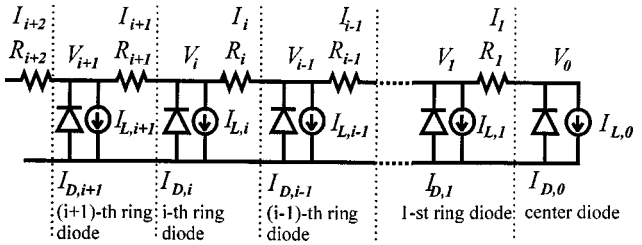

FIG. 4. Nomenclature used for the mathematical description of the resistive network. The voltage measured at the probe (or contact pads) is V_0.

Therefore, the spatial potential distribution under illumination is calculated by dividing the solar cell around the needle into concentric rings, each being represented in the numerical model by an individual diode and an associated (light-generated) current source. For the central diode, however, the light-generated current source has been omitted in Fig. 2 to indicate the shading effect. The concentric rings are electrically connected by the sheet resistance of the emitter, and the magnitude of the current source is proportional to both, the illumination intensity and the area of the ring. In the model, each individual diode is forward biased by the current sources, i.e., the light-generated current. Predominantly, the current source associated with the i-th ring forward biases the diode of the ith ring. However, for $i=0$ (i.e., the shaded diode under the contact), there is no light-generated current. This diode is forward biased by small amounts of current from each of the surrounding concentric rings. As these currents travel laterally through the sheet resistance towards the shaded contact in the center, the current flowing laterally increases and the voltage decreases, reaching a minimum at the contact. The resulting lateral potential distribution is shown in Fig. 3(a) for three different sheet resistances of the emitter (constant light-generated current density) and Fig. 3(b) shows the lateral potential distribution for three different light-generated current densities (constant sheet resistivity).

The biggest deviation of the voltage at the contact from the voltage in the (distant) nonshaded regions occurs for high sheet resistance and high light-generated current densities (high illumination densities) as can be seen in Figs. 3(a) and 3(b), respectively. In the extreme, the lateral voltage gradient predicted by the model becomes large and can become a significant fraction of the voltage across the junction. It might, therefore, be expected that in such a case the current flow within the bulk of the device does not occur only perpendicularly to the junction. In this case, the assumption that there is only one-dimensional current flow in the absorber region approximates reality less closely. For an accurate description, a two-dimensional simulation of the currents within the device (similar to that of Ref. 8) seems, therefore, necessary for very high illumination densities and very high sheet resistances. Nevertheless, and as is shown below, the general trends observed in the experiment are describable within the framework of the simple resistive network model used in this article.

A suitable nomenclature for the mathematical treatment of the model is indicated in Fig. 4. In Fig. 4 the central diode also has an associated current source, as it is reasonable to assume that the central diode below the contact is not completely shaded. For example, the sample is normally illuminated with an extended light source, which is much bigger than the area of the contact. Internal scattering—for example, from surface textures—further reduces the degree of shading under the contact. In Fig. 4, $I_{D,i}$ are the (dark) currents through the individual diodes in the model, which represent the ring-shaped sections of the diode as indicated in Fig. 2. These currents are the product of the area of the concentric ring A_i and the dark current density of the diode j_D, which is assumed to be uniform. That is, $I_{D,i}=A_i\times j_D=j_D\times\pi\times[(x_i+\Delta x_i)^2-x_i^2]$, with x_i being the inner diameter and Δx_i the width of the ith ring. The light-generated current in the ith ring-shaped section of the diode $I_{L,i}$ is the product of the area A_i and the light-generated current density j_L, which is also assumed to be uniform: $I_{L,i}=A_i\times j_L$. The light-generated current $I_{L,0}$ in the "central diode," i.e., below the contact, is zero for complete shading, or—for noncomplete shading—equal to some percentage of $A_0\times j_L$. (Note: in a more-refined version of this model the light-generated current of the center diode has to be subtracted from the light-generated current of the surrounding area.)

The resistance of the ith ring R_i represents the (lateral) resistance of the emitter for current passing from the outer to the inner perimeter of the ring

$$R_i=\int_{x_i}^{x_i+\Delta x_i}\frac{\rho dr}{2\pi r d}=\frac{\rho}{2\pi d}\ln\left(\frac{x_i+\Delta x_i}{x_i}\right)\overset{\Delta x_i\ll x_i}{\approx}\frac{\rho}{2\pi d}\frac{\Delta x_i}{x_i}, \tag{3}$$

where ρ is the specific resistivity of the emitter and d the thickness of the emitter. The voltage V_i across the individual diodes in the model have to fulfil Kirchhoff's rule as given in Eqs. 4(a) and 4(b), in which open-circuit conditions are assumed, i.e., no flow of external currents. The voltage measured by the voltmeter at the probe/contact is V_0.

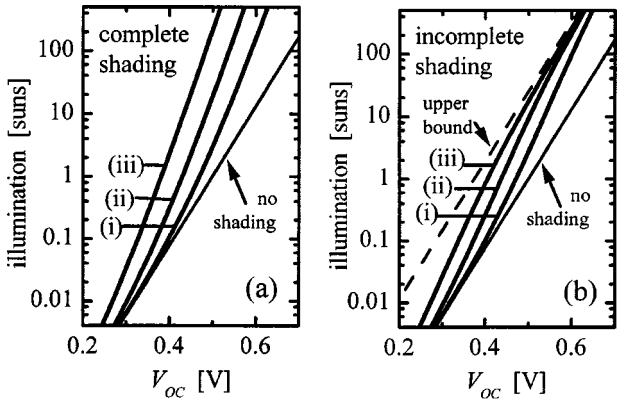

FIG. 5. Impact of contact shading in combination with high sheet resistance on Suns–V_{oc} measurements. Shown are calculated curves using the parameters given in Table I. (b) In the shaded region an average light-generated current density of 5% of that in the surrounding (nonshaded) area is assumed.

$$I_{L,i}-I_{D,i}=I_i-I_{i+1}=\frac{V_i-V_{i-1}}{R_i}-\frac{V_{i+1}-V_i}{R_{i+1}} \quad \text{for} \quad i>0, \tag{4a}$$

$$I_{L,0}-I_{D,0}=-I_1=\frac{V_0-V_1}{R_1}. \tag{4b}$$

The boundary condition for solving this problem is given in Eq. (5), whereby Eq. 5(a) applies to a finite sample size and Eq. 5(b) to a laterally infinitely extended sample:

$$\sum_i I_{D,i}=\sum_i I_{L,i} \quad \text{and} \quad |V_{i+1}-V_i|<|V_i-V_{i-1}|, \tag{5a}$$

$$V_i-V_{i-1} \xrightarrow{i\to\infty} 0. \tag{5b}$$

If the shaded contact region is small compared to the total sample area the voltage gradient virtually vanishes at sufficient distance from the contacted region, e.g., at the edge of the sample. That is, the open-circuit voltage (V_{oc}) as measured without influence from shading is present at the edges.

B. Modelling results

Figure 5 shows calculated Suns–V_{oc} curves for different degrees of contact shading. The parameters used for these calculations are given in Table I. Figure 5(a) corresponds to ''complete shading,'' i.e., no current generation under the contact, and Fig. 5(b) to ''incomplete shading,'' in which case there is a small amount of current generated below the contact (5% of the light-generated current density of the surrounding area). For comparison, each figure contains the Suns–V_{oc} curve as it would be measured without shading and sheet resistance effects (curve labeled with ''no shading''). That is, the Suns–V_{oc} of the solar cell contacted with a transparent contact (for example, a transparent conductive oxide) or with an emitter of negligible sheet resistance. The open-circuit voltage measured with a transparent contact will be referred to as ''ideal V_{oc}.'' The three bold curves in each graph of Fig. 5 correspond to three different sizes of the shaded contact region while keeping the sheet resistance constant. The simulation parameters are given in parameter set I in Table I. Interestingly, exactly the same curves can also be generated by using parameter set II in Table I, that is by using three different sheet resistances and keeping the shaded area constant. With respect to the measured Suns–V_{oc} curve and its distortion by the combination of contact shading and high sheet resistance, increasing the area of the shaded region is equivalent in the resistive network model to increasing the sheet resistance. That is, with R_{sheet} being the sheet resistance ($=\rho/d$) and r_0 the radius of the shaded region, all combinations of R_{sheet} and r_0 fulfilling $r_0^2\times R_{sheet}=$constant cause exactly the same distortion of the measured Sun–V_{oc} curve in the resistive network model.

TABLE I. Simulation parameter sets giving the Suns–V_{oc} curves of Fig. 5. In both cases is the diode ideality factor 1.6 and the light-generated current density at 1 Sun is 15 mA/cm^2.

	Parameter set I	Parameter set II
$R_{sheet}(\Omega/sq)$	3×10^7	(i) 1.2×10^6 (ii) 3×10^7 (iii) 7.5×10^8
Radius of shaded area (μm)	(i) 10 (ii) 50 (iii) 250	50

In Fig. 5(b) the three simulated curves have an upper bound, indicated by a dashed line in the graph. This curve corresponds to the voltage, which would develop in the diode directly under the contact due to its own light-generated current from the incomplete shading (that is, without any contribution from any of the surrounding ring-shaped sections of the solar cell). Note: for parameter set I, i.e., when attributing the differently shaped curves to differently sized shaded areas, this upper bound would in an experiment normally change as well with the area size of the shading contact, as the non-zero (average) light-generated current density in the volume underneath the contact stems only from an edge effect of the incomplete shading. In the calculations presented in Fig. 5(b), however, for all three curves the light-generated current density below the contact is 5% of that in the surrounding area, regardless of the area of the shading contact.

As can be seen from Fig. 5, the distortion of the Suns–V_{oc} curves due to contact shading is severe for the chosen set of parameters. The sheet resistances given in Table I appear extremely high from the perspective of crystalline Si solar cells. However, they resemble rather low sheet resistance values for amorphous Si emitters as used for example in *a*-Si:H thin-film solar cells. Furthermore, the shaded areas are not large and are well within the range of typical needle-shaped probes for voltage measurements. Nevertheless, it can clearly be seen from Fig. 5 that significant deviations from the nonshaded (ideal) V_{oc} can occur for contact shading in combination with high sheet resistances as found in thin *a*-Si:H emitters. The deviation does not simply cause a parallel shift of the Suns–V_{oc} curve (''pseudo $I-V$ curve''), but instead distorts the shape of the curve. The latter bears the danger of an erroneous assessment of the fundamental diode properties.

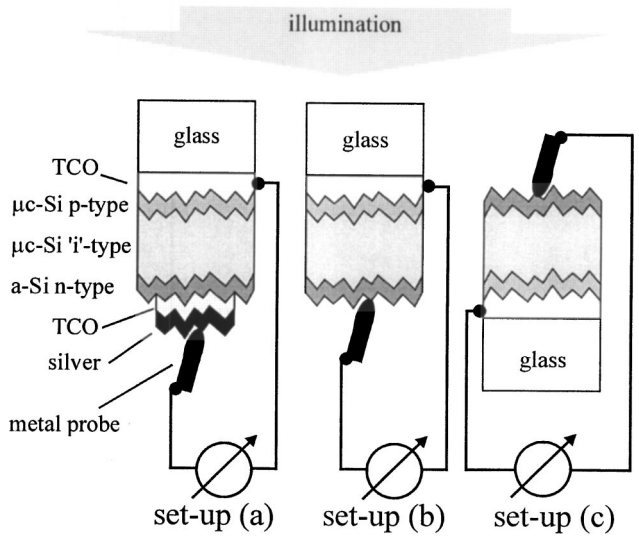

FIG. 6. Three different modes of illumination used in the measurements of the Suns–V_{oc} data displayed in Fig. 7.

The ideality factor [see Eqs. (1) and (2)] used in these calculations for each individual diode in the resistive network does not correspond to the simple analytical description or the often-used ''two-diode model.'' The value of 1.6 was used as it corresponds to the experimentally obtained curve discussed in the next section.

III. EXPERIMENTS AND COMPARISON TO MODEL

Suns–V_{oc} measurements were performed on a hydrogenated microcrystalline silicon (μc-Si:H) thin-film $p-i-n$ solar cell made on Corning 1737 glass by plasma-enhanced chemical vapor deposition at a substrate temperature of 200 °C. Apart from the hydrogen dilution of the silane gas during deposition of the i layer (higher than that for achieving the highest μc-Si:H solar cell energy conversion efficiency) the deposition conditions were similar to that of the solar cells of Refs. 5 and 6. The $p-i-n$ junction consists of three layers: ~20 nm p-type μc-Si:H, 1 μm ''intrinsic'' (not intentionally doped) μc-Si:H and ~20 nm n-type hydrogenated amorphous Si (a-Si:H). For the μc-Si:H layers a plasma excitation frequency of 94.7 MHz was used and 13.56 MHz for the a-Si:H layer. The Suns–V_{oc} characterization was done using three different ways of contacting and illuminating the sample (Fig. 6). Setup (a) in Fig. 6 is the normal contacting scheme, which is optimized with respect to the energy-conversion efficiency of μc silicon $p-i-n$ thin-film solar cells. The transparent conductive oxide (TCO) in combination with the silver pad provides a good ohmic contact and an efficient back reflector. In this way of contacting and under illumination with an intensity of 1 Sun the solar cell has an open-circuit voltage of 512 mV and an energy conversion efficiency of 6.6%. In setup (b) contact is made by directly pressing a contacting probe onto the n layer and the illumination occurs from the same side as in setup (a). In setup (c) the same contacting scheme is used as in setup (b), however, the illumination occurs from the opposite side. That is, in setup (c) the metal probe for contacting the n-type layer (emitter) locally shades the diode. Contacting

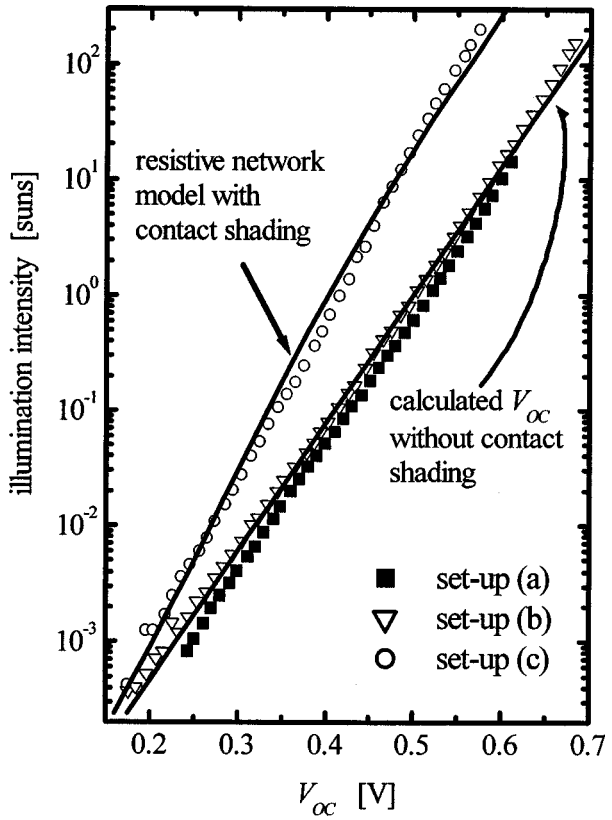

FIG. 7. Suns–V_{oc} characteristics of the μc-Si:H $p-i-n$ thin-film solar cell as measured in the three configurations shown in Fig. 6. Symbols ■, σ, and ○ correspond to the configurations shown in Figs. 6(a), 6(b), and 6(c), respectively.

the a-Si:H layer directly, as shown in Figs. 6(b) and 6(c), causes a high contact resistance. An upper bound of ~15 MΩ was determined for this contact resistance by measuring the resistance between two probes contacting the a-Si:H layer. Therefore, we used a high-impedance (~10^{12} Ω) voltage follower as a preamplifier for accurately measuring the voltage in the presence of this high contact resistance.

Figure 7 shows the Suns–V_{oc} curves obtained from measurements using the three setups shown in Fig. 6. As can be seen from the comparison of the curves corresponding to the setups (a) and (b) in Fig. 7, the use of the preamplifier allows the measurement of the open-circuit voltage even in the presence of the high contact resistance between the amorphous n-type silicon layer and the metal probe. The remaining small difference between the two curves is most likely only due to a less effective light trapping in case (b) (no backreflector). However, the curve obtained using setup (c), in which the contacting probe shades the solar cell locally, has a distinctively different shape compared to curves (a) and (b). The spectrum of the flashlight has its main intensity in the range of long wavelengths with more than 50% of the usable photons ($h\nu > 1.124$ eV) having wavelengths longer than 800 nm and almost 80% longer than 600 nm, leading to a very uniform absorption in μc-Si:H thin-film solar cells.[9] Furthermore, it has been shown in previous work[6] that the $I-V$ curves and spectral response of p-side illuminated μc-Si:H $p-i-n$ solar cells is almost identical to n-side illuminated $n-i-p$ cells. The substantial difference between

curve (c) and curves (a) and (b) can, therefore, not be ascribed to a different (vertical) generation profile. Laterally, however, there is a difference in illumination between cases (b) and (c) due to the shadow of the (needle-shaped) probe used for contacting the solar cell in case (c).

An ideality factor of 1.6 closely approximates the diode characteristics of curve (b) (see the lower solid line in Fig. 7) and was, therefore, used to describe the voltage dependence of the dark current density characteristics of the diodes in the resistive network calculations described below. A discussion of such diode characteristics on the basis of detailed device simulation has been published elsewhere.[9,10] The solar cell, when contacted as in Fig. 6(a), has a 1-Sun short-circuit current density of ~20 mA/cm^2. The parallel shift of curve (b) in Fig. 7 [solar cell contacted as in Fig. 6(b)], therefore, corresponds to a light-generated current density of ~15 mA/cm^2 at 1 Sun illumination intensity. The upper solid line in Fig. 7 is calculated using the resistive network model and approximates the experimentally obtained curve (c) quite well. As the optics of the setup for measuring curve (c) in Fig. 7 [solar cell contacted as in Fig. 6(c)] reasonably closely resemble those of the setup in Fig. 6(b), this simulation used the same 1-Sun light-generated current density (15 mA/cm^2). The needle-shaped contacting probe was measured with a micrometer, giving a radius of the tip in the range 5–10 μm. Fitting the resistive network model (upper solid line in Fig. 7) to the experimental data obtained with setup (c), therefore, yields a sheet resistance of $(2-7)\times10^{10}$ Ω/sq for the 20-nm-thick *n*-type *a*-Si:H layer. This sheet resistance value is somewhat higher, but still similar to the data reported for typical 20-nm-thick *n*-type *a*-Si:H layers in *p–i–n* Si thin-film solar cells ($\sim5\times10^9$ Ω/sq).[11] For achieving the fit to high-illumination-intensity range of the experimental data with the resistive network model, a nonzero average light-generated current density below the shading contact (5% of that in the surrounding region) has been assumed.

The simulated curve (upper solid line in Fig. 7) is a reasonable approximation to the experimental data and qualitatively explains both, (a) the deviation of the measured voltage from the ideal V_{oc} and (b) the tendency of the measured Suns–V_{oc} curve at higher intensities to become parallel to the ideal Suns–V_{oc} curve (as measured with transparent front contact or low sheet resistance).

The sheet resistance range obtained from fitting the experimental data with the theoretical model is relatively close to conductivity values that are typical for 20-nm-thick *n*-type *a*-Si:H layers in thin-film *p–i–n* Si solar cells. It, therefore, seems that the simple resistive network model is adequate for explaining the deviation of the open-circuit voltage measured in the presence of contact shading and high sheet resistance from the ideal V_{oc}. The remaining differences between the experimental and the calculated curves can possibly be reduced by a more refined model, potentially allowing for two-dimensional current flows in the bulk of the device or a refined description of shading and light-generated current density in the vicinity of the metal probe.

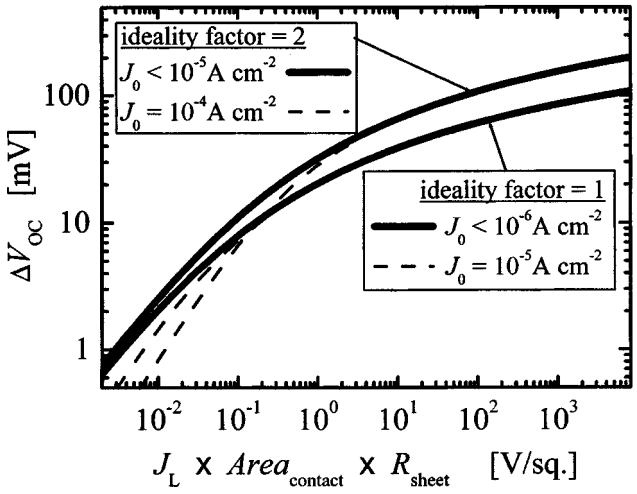

FIG. 8. Deviation ΔV_{oc} of the measured open-circuit voltage from the "ideal V_{oc}," plotted as a function of the product of the light-generated current density J_L, the emitter sheet resistance R_{sheet}, and the size of the (disk-shaped) contact area. ΔV_{oc} depends only very weakly on the saturation current density J_0 for small values of J_0.

IV. "RULE OF THUMB"

In order to provide the experimenter with a "rule of thumb" for estimating whether contact shading is likely to impact open-circuit voltage measurements on a particular solar cell, Fig. 8 shows the maximum deviation of the measured voltage from the ideal V_{oc}. The deviation (ΔV_{oc}) is plotted for different values of J_0 and two diode ideality factors as a function of the product of the light-generated current J_L, the size of the (disk-shaped) contact area, and the sheet resistance R_{sheet}. For small values of J_0 ($<10^{-5}$ A cm^{-2}, i.e., "normal" J_0 values for reasonably efficient silicon solar cells) the impact of the saturation current density on ΔV_{oc} is negligible. Only very large J_0 values alter the ΔV_{oc} appreciably, as is illustrated by the two dashed curves. For obtaining an upper limit for the deviation from the ideal V_{oc}, ΔV_{oc} is plotted under the assumption of "complete shading" of the volume below the contact as discussed in the previous sections. If light scattering produces a nonzero light-generated current in this volume, or if the diffusion length of minority charge carriers in the absorber is large compared to the lateral dimension of the shaded volume below the contact, the actual deviation from the ideal V_{oc} is smaller, as was shown for example in Fig. 5(b).

Note: The relation plotted in Fig. 8 has been calculated for disk-shaped (i.e., circular symmetry) contact areas, as in the calculations in the previous sections. Figure 8, therefore, does not describe the impact of the shading of other contact geometries (e.g., a comb-like grid structures) on V_{oc} measurements. However, as a circular disk has the lowest perimeter-to-area ratio of all geometries, using the area size of other contact geometries in Fig. 8 still provides an upper bound to the corresponding deviation ΔV_{oc} from the ideal V_{oc}.

It can be estimated from Fig. 8 that *conventional* solar cells made from crystalline Si wafers are only marginally impacted by the effect described in this article: Assuming an

emitter sheet resistance of 200 Ω/sq, and a light-generated current density of 33 mA cm^{-2}, a deviation ΔV_{oc} larger than (or equal to) 5 mV can only be expected for voltage probes with diameters larger than 1 mm.

When directly contacting an *a*-Si emitter of a Si wafer-based heterojunction solar cell such as the heterojunction with intrinsic thin layer (HIT) structure of Sanyo,[12] Fig. 8 predicts high values of ΔV_{oc} even for small contact areas. However, it has to be noted that Fig. 8 assumes ''complete shading,'' and thus zero light-generated current density below the contact probe. For needle-shaped contacting probes the minority carrier diffusion length in high-lifetime wafers (>1 mm) is long compared to the dimension of the contacted region, leading to substantial lateral carrier diffusion from the illuminated region into the shaded region. Thus, in case of high-lifetime wafers the effective light-generated current density below the contact cannot be assumed to be close to zero for very small contact areas and the value of ΔV_{oc} predicted by Fig. 8 is, therefore, higher than what should be expected from the experiment.

However, for combinations of small carrier diffusion lengths and high sheet resistances, such as in *a*-Si:H and μc-Si:H thin-film silicon solar cells, the experiments and calculations of the preceding section show that the effect quantified in Fig. 8 significantly impacts open-circuit voltage measurements.

V. CONCLUSIONS

The measurement of the open-circuit voltage as a function of the illumination intensity (Suns–V_{oc} measurement) is a useful tool for characterizing solar cells, in most cases giving a characteristic curve (pseudo-I–V curve) virtually free of series resistance effects. Here, we have shown by means of resistive network calculations that the combination of contact shading and very high sheet resistance can significantly distort the apparent diode characteristics obtained from Suns–V_{oc} measurements. For sheet resistances typical for thin layers made of doped amorphous Si even the shade of the tip of a needle-shaped contacting probe can be sufficient to cause a distorted Suns–V_{oc} curve. Suns–V_{oc} experiments were performed on a microcrystalline silicon thin-film solar cell. These show, in the presence of contact shading and large sheet resistance, significant deviations from the fundamental diode characteristics. The resistive network model qualitatively explains these deviations. The deviations not only cause a shift of the Suns–V_{oc} curve, but also result in a distortion of the shape of the curve. The latter bears the danger of an erroneous assessment of the fundamental diode properties.

A rule of thumb has been presented, allowing an estimate to be made of the impact of contact shading and sheet resistance on V_{oc} measurements for arbitrary solar cells and contact area sizes. From this rule of thumb can be concluded that V_{oc} measurements on conventional Si-wafer-based solar cells are not significantly impacted by contact shading from voltage probes with a diameter smaller than 1 mm. However, for combinations of small carrier diffusion lengths and high sheet resistances, such as in *a*-Si:H and μc-Si:H thin-film Si solar cells without TCO coating, the effect described in this article significantly impacts open-circuit voltage measurements even when using very thin needle-shaped voltage probes.

ACKNOWLEDGMENTS

The authors thank A. Lambertz, O. Vetterl, A. Gross, and F. Finger from the Institute of Photovoltaics, Forschungszentrum Jülich, Germany, for sample preparation and technical support. One of the authors (N.-P.H.) gratefully acknowledges his postgraduate scholarship from the ''Evangelisches Studienwerk Villigst e.V.,'' Germany. The work described here has been supported by the Australian Research Council under the ''Large Grant'' scheme.

[1] M. Wolf and H. Rauschenbach, Adv. Energy Conversion **3**, 455 (1963).
[2] R. A. Sinton and A. Cuevas, Proceedings of the 16th E.C. PVSEC (2000), pp. 1152–1155.
[3] M. J. Kerr, A. Cuevas, and R. A. Sinton, J. Appl. Phys. **91**, 399 (2002).
[4] D. H. Neuhaus, N.-P. Harder, S. Oelting, R. Bardos, A. B. Sproul, P. Widenborg, and A. G. Aberle, Sol. Energy Mater. Sol. Cells **74**, 225 (2002).
[5] O. Vetterl, A. Lambertz, A. Dasgupta, F. Finger, B. Rech, O. Kluth, and H. Wagner, Sol. Energy Mater. Sol. Cells **66**, 345 (2001).
[6] A. Gross, O. Vetterl, A. Lambertz, F. Finger, H. Wagner, and A. Dasgupta, Appl. Phys. Lett. **79**, 2841 (2001).
[7] M. Vieira, A. Maçarico, E. Morgado, S. Koynov, and R. Schwarz, J. Non-Cryst. Solids **227-230**, 1311 (1998).
[8] A. Fantoni, M. Vieira, and R. Martins, Mater. Res. Soc. Symp. Proc. **467**, 765 (1997).
[9] T. Brammer, Ph.D. thesis, Heinrich-Heine-Universität Düsseldorf (2002); http://www.ulb.uni-duesseldorf.de/diss/mathnat/2002/brammer.html
[10] T. Brammer and H. Stiebig, J. Appl. Phys. **94**, 1035 (2003).
[11] R. E. I. Schropp and M. Zeman, *Amorphous and Microcrystalline Silicon Solar Cells: Modeling, Materials, and Device Technology* (Kluwer Academic, Boston, 1998), Table 3.4, p. 60.
[12] M. Taguchi, K. Kawamoto, S. Tsujge, T. Baba, H. Sakata, M. Morizane, K. Uchihashi, N. Nakamura, S. Kiyama, and O. Oota, Prog. Photovoltaics **8**, 503 (2000).